BULLETIN OF THE POLISH ACADEMY OF SCIENCES
TECHNICAL SCIENCES, Vol. 68, No. 5, 2020
DOI: 10.24425/bpasts.2020.134650

SPECIAL SECTION

Predictive current control of three-phase matrix converter with GaN HEMT bidirectional switches

K. NOWASZEWSKI* and A. SIKORSKI

Department of Power Electronics and Electric Drives, Bialystok University of Technology, ul. Wiejska 45D, 15-351 Bialystok, Poland

Abstract. This paper presents an analysis and simulation studies of three-phase matrix converter with GaN HEMT bidirectional switches with predictive control of grid currents and converter output currents. Two methods of grid currents shaping are described and compared. The first method is based on calculations of instantaneous grid reactive power and the second one uses the active power of the load. The analyzed converter works with the resistive-inductive load, and from the grid side the LC filter with damping resistor has been used.

Key words: predictive control, matrix converter, GaN HEMT, LC filter, bidirectional switch.

1. Introduction

The matrix converter (MC) is an AC/AC type converter which converts directly (without a DC voltage stage) alternating voltage to alternating voltage with variable amplitude and frequency. The MC also allows for bidirectional electric energy transfer with power factor correction [1].

An extensive review of MC control methods has been presented in [2], scalar methods [3], PWM/SVM [4], DTC [5] and predictive control, among others. Predictive methods are used in torque [6, 7] and current control [8]. The cost function at predictive control could contain many parameters, which will affect the shape of the currents, e.g. instantaneous grid reactive power, current deviations, or common-mode voltage. Due to the possibility of wide parameters selection in the cost function, increase signal processors computing power [9] and the possibility of implementation of the predictive control in the FPGA systems [10] interest in predictive control shows a significant increase. The application of GaN HEMTs as a bidirectional switch in the MC [11] facilitates switching frequency and power density increase (however, the possibility of an increase in power losses in reverse conduction mode of GaN HEMT should be taken into account [12]).

2. Predictive input currents control based on instantaneous reactive power (method I – based on [13])

2.1. Model. The three-phase MC consists of 9 bidirectional switches S_{ij}, which connect each input phase with each output phase (Fig. 1). An L_fC_f lowpass filter with a damping resistor R_d was used at the converter input. The converter has been loaded with an RL circuit. An inseparable part of the MC is a clamping circuit (Fig. 2), connected to the inputs and outputs of the MC, which protects the converter against overvoltage from grid or load side caused by wrong current direction detection during the semi-soft commutation process or by unexpected interruption of load current [1].

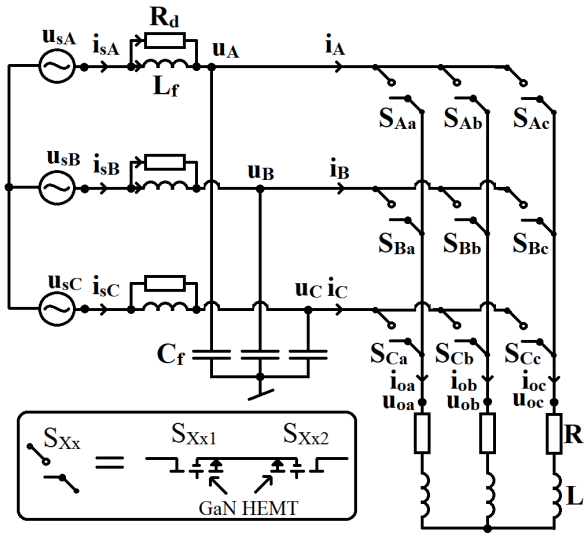

Fig. 1. Three-phase matrix converter with input filter L_fC_f and damping resistor R_d with RL load

To describe the relationship between input and output variables, instantaneous transfer matrices S_{ij} and S'_{ij} are defined as

$$S_{ij} = \begin{pmatrix} S_{Aa} & S_{Ba} & S_{Ca} \\ S_{Ab} & S_{Bb} & S_{Cb} \\ S_{Ac} & S_{Bc} & S_{Cc} \end{pmatrix}, \quad S'_{ij} = \begin{pmatrix} S_{Ab} & S_{Bb} & S_{Cb} \\ S_{Ac} & S_{Bc} & S_{Cc} \\ S_{Aa} & S_{Ba} & S_{Ca} \end{pmatrix}. \quad (1)$$

*e-mail: k.nowaszewski@doktoranci.pb.edu.pl

Manuscript submitted 2020-05-13, revised 2020-07-30, initially accepted for publication 2020-08-04, published in October 2020

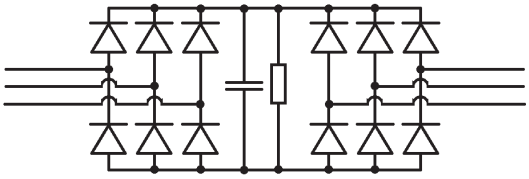

Fig. 2. Protective clamping circuit

An instantaneous transfer matrix S_{ij} can have 27 different possible combinations [1] with respect to the following rules:

- Input phases cannot be shorted.
- Circuits of the output currents cannot be interrupted.

A S'_{ij} matrix is a modification of S_{ij} needed for calculation. To simplify the calculations, the following voltage and current matrices are introduced:

$$i_s = \begin{pmatrix} i_{sA} \\ i_{sB} \\ i_{sC} \end{pmatrix}, \quad u_s = \begin{pmatrix} u_{sA} \\ u_{sB} \\ u_{sC} \end{pmatrix}, \quad i = \begin{pmatrix} i_A \\ i_B \\ i_C \end{pmatrix}, \quad u = \begin{pmatrix} u_A \\ u_B \\ u_C \end{pmatrix} \tag{2}$$

$$i_o = \begin{pmatrix} i_{oa} \\ i_{ob} \\ i_{oc} \end{pmatrix}, \quad u_o = \begin{pmatrix} u_{oa} \\ u_{ob} \\ u_{oc} \end{pmatrix}, \quad u_{o-pp} = \begin{pmatrix} u_{oab} \\ u_{obc} \\ u_{oca} \end{pmatrix}. \tag{3}$$

The relationship between the input/output currents and voltages that make up the MC model is defined as follows:

$$i = S_{ij}^T i_o\,, \tag{4}$$

$$u_o = \frac{1}{3}\begin{bmatrix} u_{oab} - u_{oca} \\ u_{obc} - u_{oab} \\ u_{oca} - u_{obc} \end{bmatrix}, \qquad u_{o-pp} = \left(S_{ij} - S'_{ij}\right) u = S_{ij-pp} u. \tag{5}$$

The scheme of MC predictive control is shown in Fig. 3. Predictive control relies on the calculation of 27 different possible

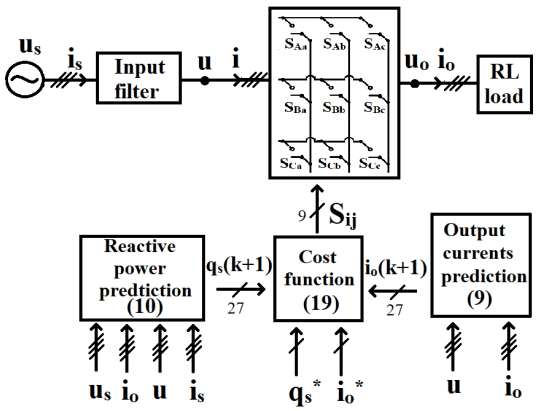

Fig. 3. Scheme of matrix converter predictive current control with instantaneous reactive power prediction

errors of reactive power and errors of output currents in the next sampling step $k+1$ based on selected measured values at the moment k and reference output current value. For this purpose, a discrete form of equation is used with a sampling period T_p. Then, the modules of those errors are added together for each state of instantaneous transfer matrix S_{ij} and the cost function selects the minimum value of that sum. That minimum value of the sum corresponds to the 1 of 27 states of S_{ij}, which will be used.

To determine the values of the output currents at the moment $k+1$, the voltage equation for the output circuit in the time form could be written

$$u_o(t) = Ri_o(t) + L\frac{di_o(t)}{dt}\,, \tag{6}$$

and the discrete form of this equation

$$\frac{u_o(k+1)+u_o(k)}{2} = R\frac{i_o(k+1)+i_o(k)}{2} + L\frac{i_o(k+1)-i_o(k)}{T_p}\,. \tag{7}$$

The discrete form for the moment k is obtained by using forward Euler approximation

$$\frac{di_o(t)}{dt} \approx \frac{i_o(k+1)-i_o(k)}{T_p}\,, \tag{8}$$

with a modification which includes that on current in the inductor acts as a mean value of the voltage. Using Eq. (7) $i_o(k+1)$ is obtained

$$i_o(k+1) = \frac{2T_p}{2L+RT_p}\frac{u_o(k+1)+u_o(k)}{2} - \frac{2L-RT_p}{2L+RT_p} i_o(k). \tag{9}$$

Based on the above equation, 27 possible values of the output current at $k+1$ can be determined. The values $u_o(k)$ and $u_o(k+1)$ are calculated using Eqs. (5) and (16).

To determine the reactive power at $k+1$, the following equation is used, in which the currents and voltages of the network have been transferred to the $\alpha\beta$ stationary system

$$q_s(k+1) = u_{s\alpha}(k+1)i_{s\beta}(k+1) - u_{s\beta}(k+1)i_{s\alpha}(k+1). \tag{10}$$

The voltage $u_s(k+1)$ was estimated using Lagrange interpolation [13], because it is a slow-changing waveform in relation to the sampling time. To determine the grid currents at $k+1$, the voltage and current equation of the input circuit was used as state space model

$$\begin{bmatrix} \dfrac{du(t)}{dt} \\ \dfrac{di_{L_f}(t)}{dt} \\ 0 \end{bmatrix} = A_c \begin{bmatrix} u(t) \\ i_{L_f}(t) \\ 0 \end{bmatrix} + B_c \begin{bmatrix} u_s(t) \\ i(t) \\ i_{R_d}(t) \end{bmatrix}, \tag{11}$$

where

$$A_c = \begin{bmatrix} 0 & \frac{1}{C_f} & 0 \\ -\frac{1}{L_f} & 0 & 0 \\ \frac{1}{R_d} & 0 & 0 \end{bmatrix}, \quad B_c = \begin{bmatrix} 0 & -\frac{1}{C_f} & \frac{1}{C_f} \\ \frac{1}{L_f} & 0 & 0 \\ -\frac{1}{R_d} & 0 & 1 \end{bmatrix}. \quad (12)$$

The zero-order hold (ZOH) discrete form is

$$\begin{bmatrix} u(k+1) \\ i_{L_f}(k+1) \\ 0 \end{bmatrix} = A_d \begin{bmatrix} u(k) \\ i_{L_f}(k) \\ 0 \end{bmatrix} + B_d \begin{bmatrix} u_s(k) \\ i(k) \\ i_{R_d}(k) \end{bmatrix}, \quad (13)$$

and the A_d and the B_d was obtained by using second-order approximation of the exact solution

$$A_d = I + A_c T_p + \frac{A_c^2 T_p^2}{2}, \quad B_d = \left(T_p I + \frac{A_c T_p^2}{2} \right) B_c. \quad (14)$$

From (13), (4) and (5) we can obtain

$$i_{L_f}(k+1) = n_1 u(k) + n_2 i_{L_f}(k) + n_3 u_s(k) + n_4 S_{ij}^T i_o(k) + n_5 i_{R_d}(k), \quad (15)$$

$$u(k+1) = m_1 u(k) + m_2 i_{L_f}(k) + m_3 u_s(k) + m_4 S_{ij}^T i_o(k) + m_5 i_{R_d}(k). \quad (16)$$

where $n_1 \div n_5$ and $m_1 \div m_5$ are coefficients whose values result from the above transformations. The damping resistor current i_{Rd} at $k+1$ is calculated using the equation below

$$i_{R_d}(k+1) = \frac{u_s(k+1) - u(k+1)}{R_d}. \quad (17)$$

The source current i_s is the sum of i_{Lf} and i_{Rd} so

$$i_s(k+1) = i_{R_d}(k+1) + i_{L_f}(k+1). \quad (18)$$

Having derived the final form for the grid current in the next step (18), now its value can be calculated for 27 different combinations and as a result it is possible to calculate 27 reactive power values at the moment $k+1$.

The cost function takes the following form

$$J = \Delta i_o(k+1) + w \Delta q_s(k+1), \quad (19)$$

where

$$\Delta i_o(k+1) = |i_o^* - i_o(k+1)|, \quad (20)$$

$$\Delta q_s(k+1) = |q_s^* - q_s(k+1)|, \quad (21)$$

w is the reactive power weighting factor expressed in V^{-1} units, and i_o^* is the matrix 3×1 with reference sinusoidal output currents with amplitude I_{om}^*, while q_s^* is the reference reactive power of the grid.

2.2. Simulation studies. In order to verify the predictive current control presented in the previous section, simulation tests were performed in the *Matlab/Simulink* environment with *PSpice SLPS* interface, which enabled use of the real model of the *GS66506T* transistor. The parameters of the tested system are in Table 1. The input filter uses a damping resistor R_d, connected in parallel to the L_f choke, suppressing the resonance frequency of the $L_f C_f$ filter. The 4-step current commutation method has been used with 200 ns dead time. The simulation was performed with RL load.

Table 1
Matrix converter parameters with RL load and LC input filter

Parameter name	Symbol	Value
Filtering choke	L_f	300 µH
Filtering capacitor	C_f	30 µF
Filter resonance frequency ($L_f C_f$)	f_r	1.6 kHz
Damping resistor	R_d	9 Ω
Load resistor	R	5.6 Ω
Load choke	L	3.5 mH
Sampling time	T_p	10 µs
RMS of grid voltage	U_s	230 V
Frequency of grid voltage	f_s	50 Hz
Drain to source resistance of GS66506T at on state	$R_{DS(on)}$	67 mΩ

Fig. 4 presents output voltage and output current of phase a waveforms as well as phase A grid voltage and current waveforms during a converter operation with the reference output current amplitude $I_{om}^* = 15$ A at frequency $f_o^* = 30$ Hz, reference reactive power $q_s^* = 0$ var and a weighting factor w equals 0 V^{-1}. The output current waveform is shaped as intended – due to proper prediction THD of i_{oa} current equals 1.29%. By zeroing the weighting factor, reactive power control is disabled, which can be seen from the distorted current waveform. The average switching frequency in this case was about 41.1 kHz (while the maximum switching frequency, resulting from the sampling time is 100 kHz), and the converter efficiency (including input filter and clamping circuit) was 94.3%.

Fig. 5 shows the same waveforms, but the reactive power weighting factor has been changed to 0.01 V^{-1}. That value was initially estimated based on the ratio of current to reactive power $q = 3U_m i = 3\sqrt{2}U_{rms} i = 3\sqrt{2} \cdot 230\, i \approx 976i \rightarrow$ $\rightarrow w = \frac{i}{q} \approx 0.001$ V^{-1}. Then the optimal value of the w factor, from the current THD point of view, was determined experimentally. It can be seen that the correct selection of the weighting factor ensured an almost sinusoidal mains current in the phase with mains voltage, so the system compensates reactive power. The THD of i_{oa} current equals 1.98% and THD of i_{sA} current equals 6.17%. In this case, the average switching frequency increased to about 59.95 kHz. The converter effi-

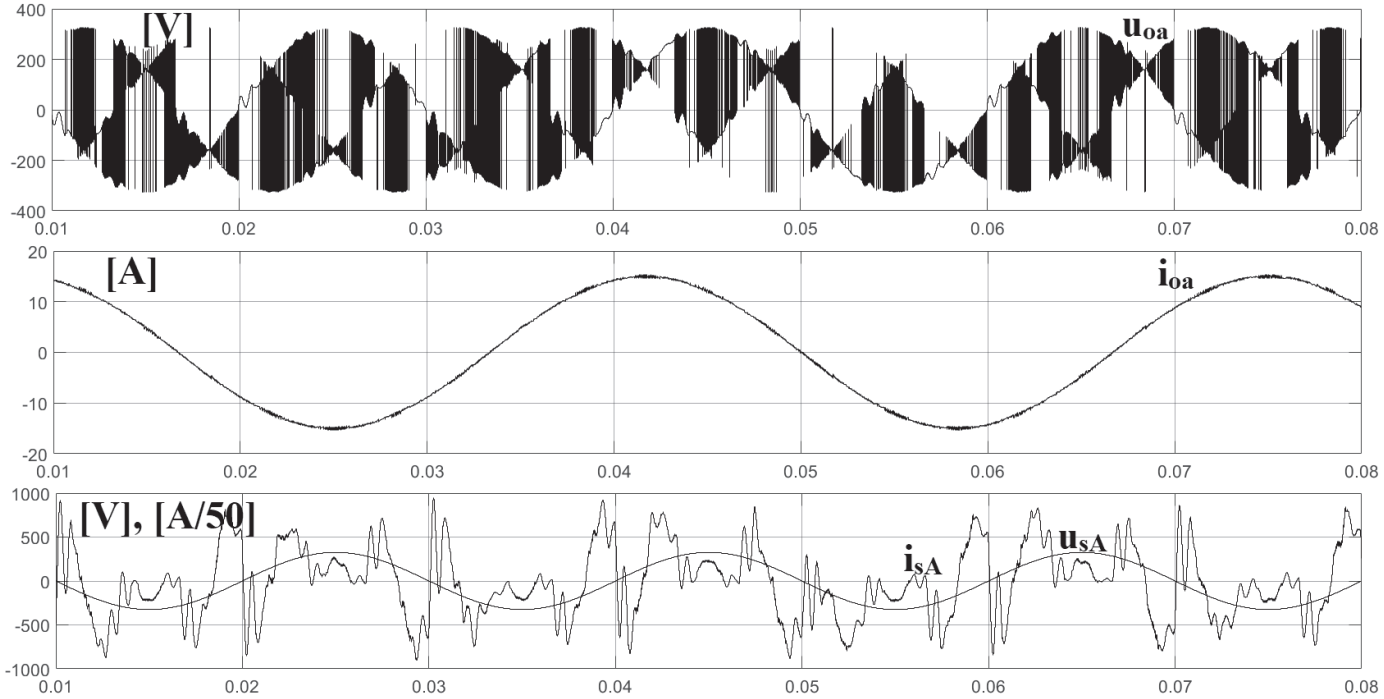

Fig. 4. MC waveforms during work with: $I^*_{om} = 15$ A, $q^*_s = 0$ var, $w = 0$ V^{-1}, $f^*_o = 30$ Hz

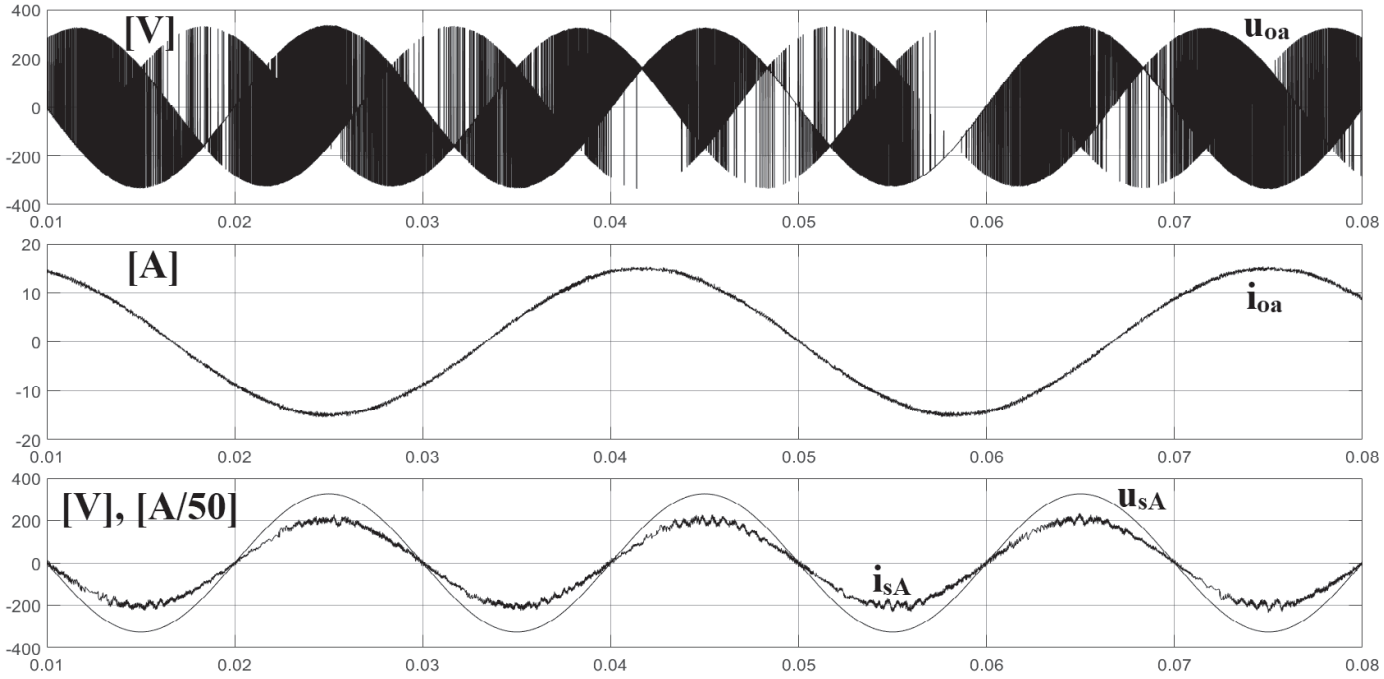

Fig. 5. MC waveforms during work with: $I^*_{om} = 15$ A, $q^*_s = 0$ var, $w = 0.01$ V^{-1}, $f^*_o = 30$ Hz

ciency was up to 94.4%, so increase in switching frequency by 18.85 kHz did not cause a significant change in the converter efficiency.

Figs. 6, 7 and 8 present waveforms of mains currents and voltages, output currents for the reference value of output current $I^*_{om} = 15$ A, reference reactive power $q^*_s = 0$ var for the frequency f^*_o: 30 Hz, 50 Hz and 70 Hz. The change in frequency from 30 Hz to 50 Hz resulted in a decrease in the total harmonic distortion ratio THD of i_{sA} current from 6.17% to 5.23%, but at 70 Hz the THD was equal to 6.14%. The THD of i_{oa} current was 1.98%, 1.84% and 1.94% for 30 Hz, 50 Hz and 70 Hz, respectively.

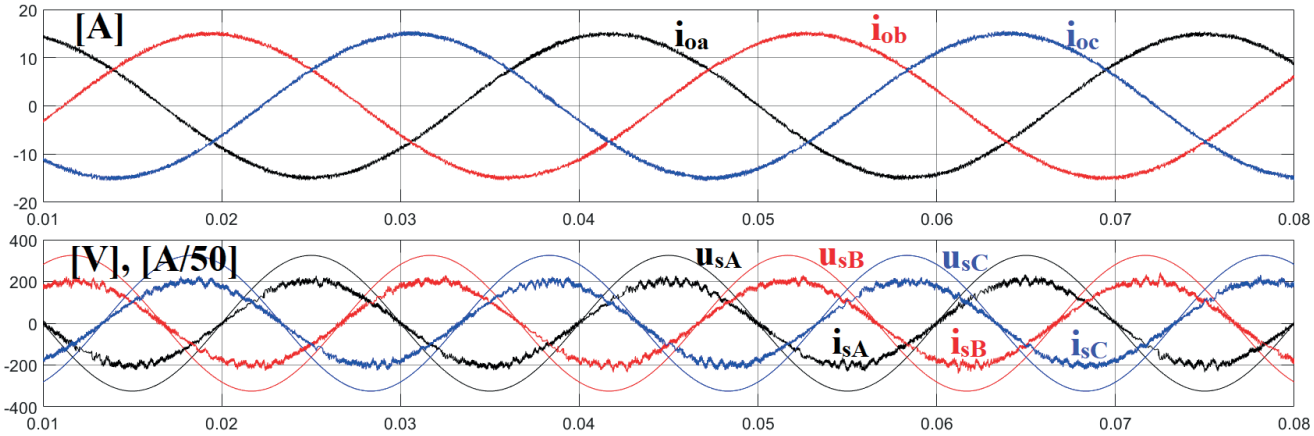

Fig. 6. MC waveforms during work with: $I^*_{om} = 15$ A, $q^*_s = 0$ var, $w = 0.01$ V^{-1}, $f^*_o = 30$ Hz

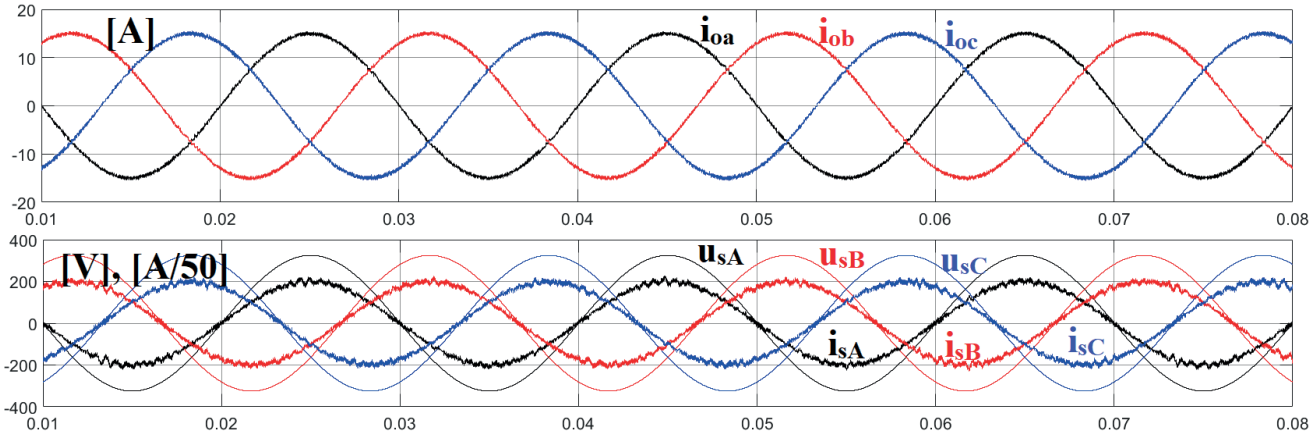

Fig. 7. MC waveforms during work with: $I^*_{om} = 15$ A, $q^*_s = 0$ var, $w = 0.01$ V^{-1}, $f^*_o = 50$ Hz

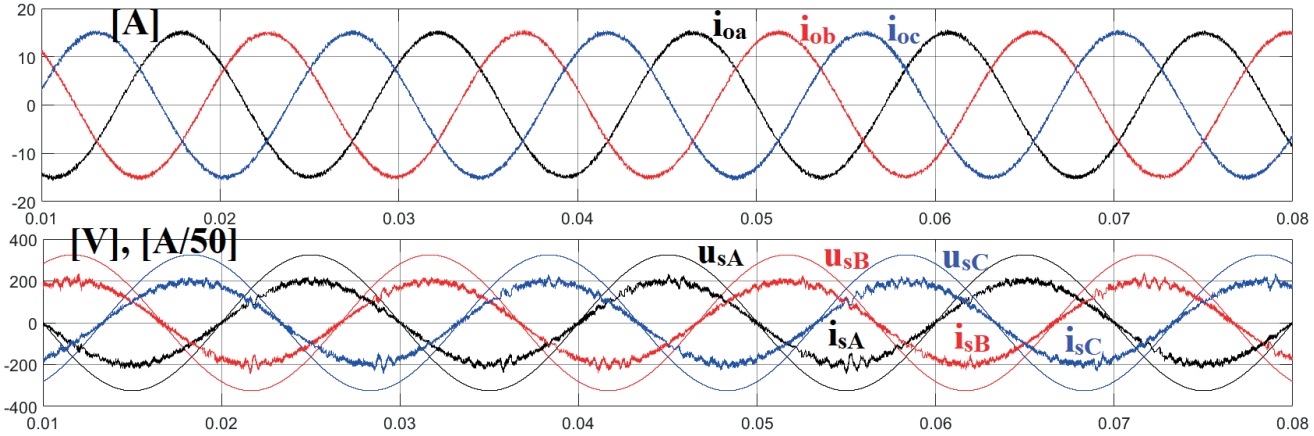

Fig. 8. MC waveforms during work with: $I^*_{om} = 15$ A, $q^*_s = 0$ var, $w = 0.01$ V^{-1}, $f^*_o = 70$ Hz

3. Predictive input currents control based on active power (method II)

3.1. Model. Another method which was investigated during the research is a prediction of reference input currents based on load active power calculation. The reference RMS value of the input currents is calculated as follows

$$I^*_s = \frac{RI^{*2}_o}{U_s \cos\varphi^* \eta}, \tag{22}$$

where P_s is the active power of the three-phase load, I^*_o is the RMS value of reference output current, η is the MC efficiency

which is variable and depends on the load power P_{load} and the effective switching frequency f_{sw}. The instantaneous reference values of input currents are shaped as a sinus function with input voltage phase angle, e.g. for phase A the reference current is calculated based on the following equation

$$i^*_{sA}(t+T_p) = \sqrt{2} I^*_s \sin\left[\omega_s (t+T_p) - \varphi^*\right], \tag{23}$$

where ω_s is the pulsation of the phase A grid voltage and the φ^* is the reference angle between the reference grid current and the grid voltage, to regulate the grid reactive power. The scheme of this control is present in Fig. 9.

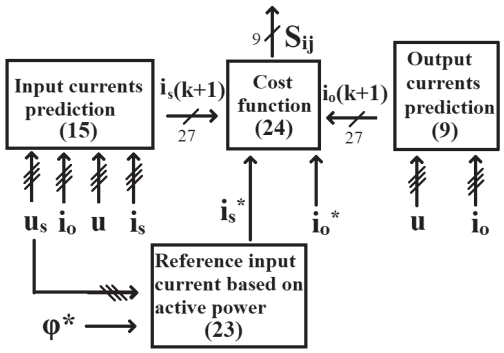

Fig. 9. Scheme of matrix converter predictive curent control based on active power of the load

Due to the change of reference parameter, the cost function has also changed to

$$J_{i_s} = \Delta i_o(k+1) + w_{i_s} \Delta i_s(k+1), \tag{24}$$

where

$$\Delta i_s(k+1) = \left| i^*_s(k+1) - i_s(k+1) \right|, \tag{25}$$

and the w_{is} is the weighting factor of $\Delta i_s(k+1)$. The rest of the calculation is the same as in the first method.

3.2. Simulation studies. The simulation was performed with identical system parameters as in the first method (Table 1) and for: $I^*_o = 15$ A, $\varphi^* = 0$ rad/s, $w_{is} = 2$, $\eta = 0.94$ and $f^*_o = 30$ Hz. The results are presented in Fig. 10. In comparison to the first method, the *THD* of phase A grid current i_{sA} is 2.06% lower and equals 4.11%. The THD of i_{oa} current is similar and equals 1.93%. It could be seen that the oscilations caused by resonance frequency of input filter are much smaller. The average switching frequency in that case increases by about approximately 3.14 kHz in reference to method I and equals 63.09 kHz.

4. Methods comparison

The assessment of method II has been done in reference to method I and the following criteria:

1. Complexity of control implementation.
2. Complexity of weighting factor selection.
3. Sampling frequency.
4. Switching frequency.
5. THD of input current.
6. THD of output current.
7. Filter resonance frequency immunity.
8. Dynamic response to a current and frequency step change.
9. Reactive power control.

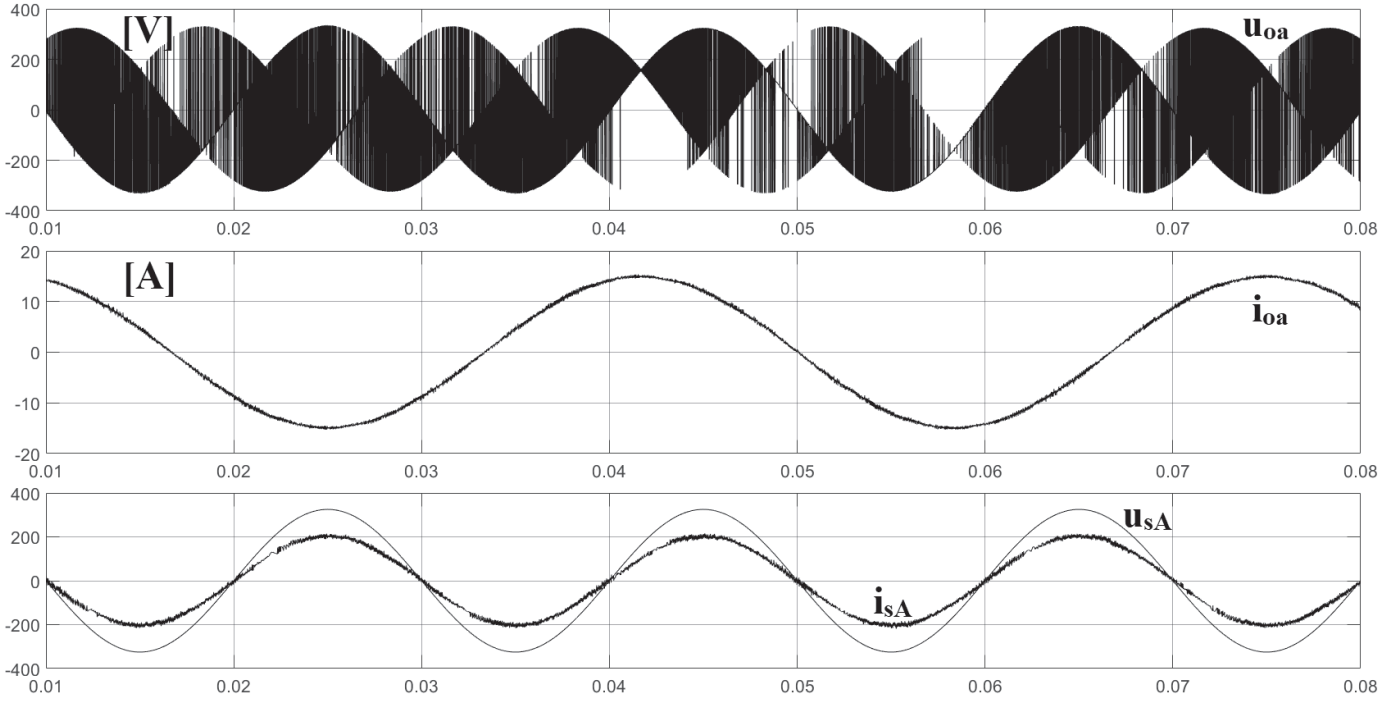

Fig. 10. MC waveforms with predictive input currents control based on active power: $I^*_{om} = 15$ A, $\varphi^* = 0$ rad/s, $w_{is} = 2$, $\eta = 0.94$ and $f^*_o = 30$ Hz

Fig. 11a presents the waveforms of MC during work with reference reactive power $q_s^* = 700$ var for method I. For method II (Fig. 11b) the phase angle $\varphi^* = 0.354$ rad/s (the value of this angle corresponds to 700 var). It can be seen that both methods facilitate reactive power control and simultaneously control the sinusoidal grid and load currents. There is a difference with setting up the value of reference reactive power. To control reactive power using method I, it is enough to insert q_s^* different from zero, but for method II it is necessary to calculate reactive power into the phase shift between the phase grid voltage and phase grid current and set the reference phase angle φ^*, but that could be easily modified by taking into account the relation between the reactive power and phase angle.

To compare the methods in dynamic state, an output current frequency and amplitude step was performed, shown in Figs. 12 and 13. During the frequency step from 30 Hz to 70 Hz there are no differences between method I and II. Output currents changed the frequency smoothly at a similar time, without disturbing grid currents. The difference between presented methods can be seen during the output current amplitude step from 15 A to −15 A. Method I changed the amplitude in 0.4 ms, but the grid currents have been distorted. Method II made this step twice as slow – in 0.8 ms, but the grid currents have not been affected.

The assessment is summarized in Table 2. The main weaknesses of method II in reference to method I is slower response

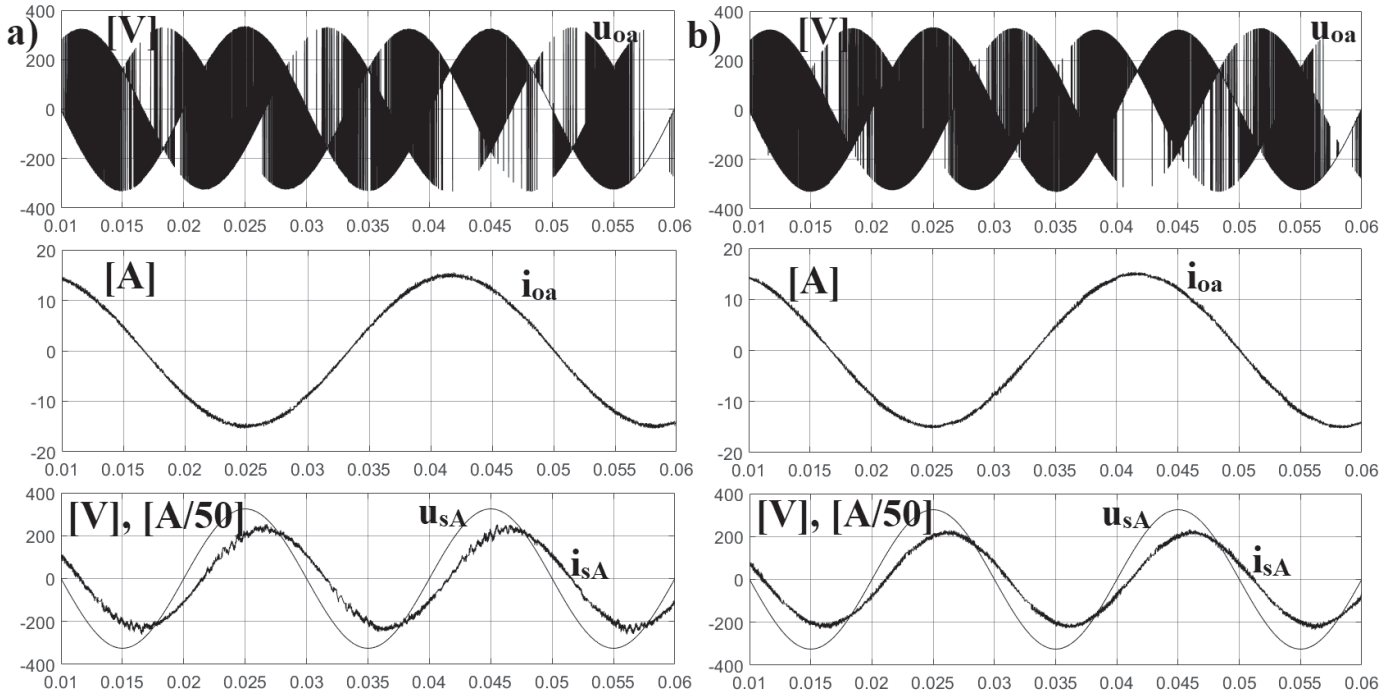

Fig. 11. MC waveforms with predictive input currents control based on: a) reactive power (method I) with: $I_{om}^* = 15$ A, $Q^* = 700$ var, $w = 0.01$ V^{-1} and $f_o^* = 30$ Hz; b) active power (method II) with: $I_{om}^* = 15$ A, $\varphi^* = 0.354$ rad/s, $w_{is} = 2$, $\eta = 0.94$ and $f_o^* = 30$ Hz

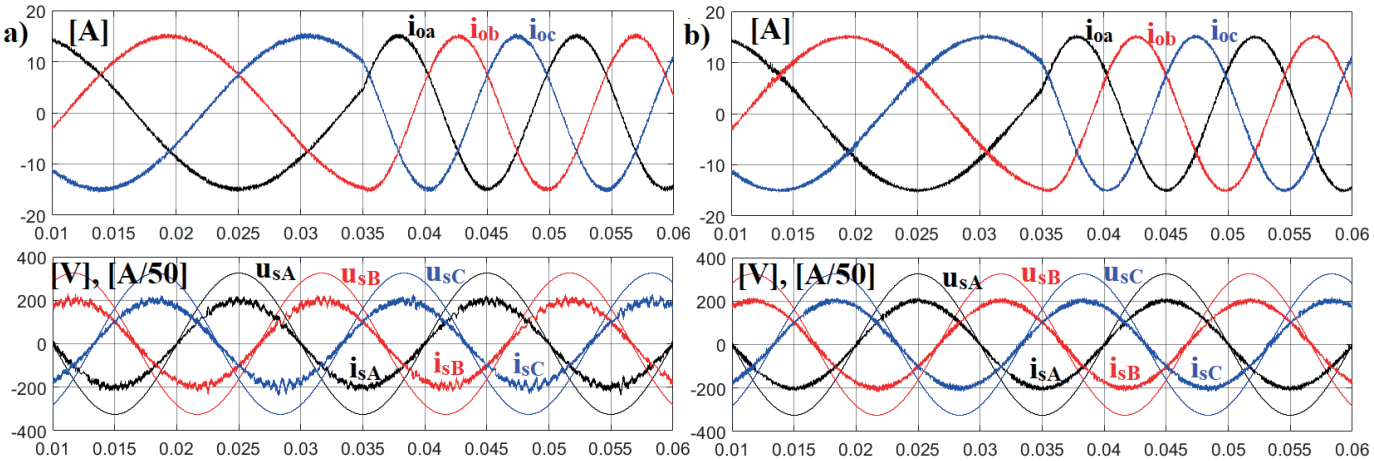

Fig. 12. MC waveforms during output current freqency step from 30 Hz to 70 Hz at 0.035 s: a) method I with: $I_{om}^* = 15$ A, $Q^* = 0$ var, $w = 0.01$ V^{-1} and $f_o^* = 30$ Hz; b) method II with: $I_{om}^* = 15$ A, $\varphi^* = 0$ rad/s, $w_{is} = 2$, $\eta = 0.94$ and $f_o^* = 30$ Hz

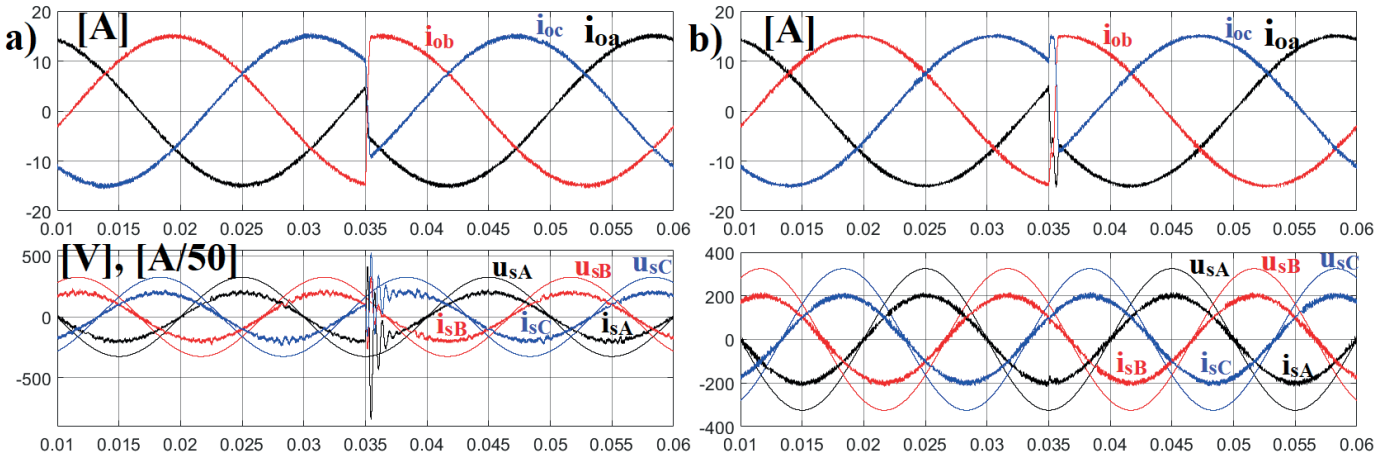

Fig. 13. MC waveforms during output current amplitude step from 15 A to −15 A at 0.035 s: a) method I with: $I^*_{om} = 15$ A, $Q^* = 0$ var, $w = 0.01$ V^{-1} and $f^*_o = 30$ Hz; b) method II with: $I^*_{om} = 15$ A, $\varphi^* = 0$ rad/s, $w_{is} = 2$, $\eta = 0.94$ and $f^*_o = 30$ Hz

Table 2
Assessment of method II in reference to method I

	Complexity of control implementation	Complexity of weighting factor selection	Switching frequency	THD of input current	THD of output current	Resonance frequency immunity	Reactive power control	Current step	Frequency step
Method II	lowest	lowest	similar	better	similar	better	similar	slower, but does not cause distortion of the grid current	similar

to output current amplitude step. Another disadvantage could be the sensitivity to efficiency changes. Despite this, method II is more attractive for less dynamic loads because of the lowest complexity of control implementation and weighting factor selection, better THD of grid currents and immunity to filter resonance frequency. In other analyzed properties, i.e. the switching frequency and THD of output current, reactive power control method II was similar to method I.

5. Summary

Simulation tests and analysis of matrix converter operation with predictive current control for both methods confirmed the effectiveness of these control methods. The first method, which was based on reactive power had a higher THD than the second method, which is based on active power. It should be noted, however, that despite the use of a damping resistor in the input filter in mains current waveforms, current oscillations can be seen at the filter resonance frequency for the first method. Therefore, the first method requires introducing some modifications, e.g. using the active damping method, to reduce more effectively occurring oscillations or adding another parameter to the cost function. While with the second method, the *THD* of i_{sA} current could drop down to 4.11%. The weighting factor was selected based on the minimum *THD* factor of the mains current. The use of GaN HEMT as bidirectional switches facilitates operation with a high switching frequency, simultaneously improves the quality of shaped currents, while the system maintains high efficiency due to very low connection losses.

Acknowledgements. This work was supported by the Ministry of Science and Higher Education in Poland under work No. MB/WE/2/2018, S/WE/1/2018 and WI/WE-IA/8/2020.

References

[1] P. Szcześniak, *Three-Phase AC–AC Power Converters Based on Matrix Converter Topology: Matrix-Reactance Frequency Converters Concept*, Springer, 2013.

[2] J. Rodriguez, M. Rivera, J.W. Kolar, and P.W. Wheeler, "A Review of Control and Modulation Methods for Matrix Converters", *IEEE Trans. Ind. Electron.* 59 (1), 58–70 (2012).

[3] M. Venturini, "A new sine wave in sine wave out, conversion technique which eliminates reactive elements", *in Proc. Powercon 7*, E3/1–E3/15 (1980).

[4] R. Wiśniewski, G. Bazydło, P. Szcześniak, and M. Wojnakowski, "Petri Net-Based Specification of Cyber-Physical Systems Oriented to Control Direct Matrix Converters With Space Vector Modulation", *IEEE Access* 7, 23407–23420 (2019).

[5] D. Casadei, G. Serra, and A. Tani, "The use of matrix converters in direct torque control of induction machines", *IEEE Trans. Ind. Electron.* 48 (6), 1057–1064 (2001).

[6] M. Rivera, R. Vargas, J. Espinoza, and J. Rodriguez, "Behavior of the predictive DTC based matrix converter under unbalanced AC-supply", *Proc. IEEE Power Electron. Spec. Conf.*, 202–207 (2007).

[7] V. Talavat, S. Galvani, and M. Hajibeigy, "Direct predictive control of asynchronous machine torque using matrix converter", *Bull. Pol. Ac.: Tech*. 67 (4), 773–788 (2018).

[8] S. Muller, U. Ammann, and S. Rees, "New time-discrete modulation scheme for matrix converters", *IEEE Trans. Ind. Electron.* 52 (6), 1607–1615 (2005).

[9] P. Falkowski, A. Sikorski, K. Kulikowski, and M. Korzeniewski, "Properties of active rectifier with LCL filter in the selection process of the weighting factors in finite control set-MPC", *Bull. Pol. Ac.: Tech*. 68 (1), 51–50 (2020).

[10] O. Gulbudack and E. Santi, "FPGA-Based Model Predictive Controller for Direct Matrix Converter", *IEEE Trans. Ind. Electron.* 63 (7), 4560–4570 (2016).

[11] K.C. Nowaszewski and A. Sikorski, "Application of GaN HEMT as a bidirectional switch in matrix converter", *Prz. Elektrotechniczny*, 2019 (8), 160–163 (2019).

[12] M. Zdanowski, and J. Rąbkowski, "Operation modes of the GaN HEMT in high-frequency half-bridge converter", in *Conference Progress in Applied Electrical Engineering PAEE 2016*, Kościelisko – Zakopane, Poland (2016), DOI: 10.1109/PAEE.2016.7605115.

[13] M. Rivera, C. Rojas, J. Rodriguez, P. Wheeler, B. Wu, and J. Espinoza, "Predictive Current Control With Input Filter Resonance Mitigation for a Direct Matrix Converter", *IEEE Trans. Ind. Electron.* 26 (10), 2794–2803 (2011), DOI: 10.1109/TPEL.2011.2121920.